Influence of stable Floquet exponents on time-delayed feedback control

Wolfram Just,[1,*] Ekkehard Reibold,[2] Krzysztof Kacperski,[2,3] Piotr Fronczak,[2,4] Janusz A. Hołyst,[3,4] and Hartmut Benner[2]
[1]*School of Mathematical Sciences, Queen Mary & Westfield College, Mile End Road, London E1 4NS, United Kingdom*
[2]*Institut für Festkörperphysik, Technische Universität Darmstadt, Hochschulstraße 6, D-64289 Darmstadt, Germany*
[3]*Max Planck Institute for Physics of Complex Systems, Nöthnitzer Straße 38, D-01187 Dresden, Germany*
[4]*Faculty of Physics, Warsaw University of Technology, Koszykowa 75, PL-00-662 Warsaw, Poland*
(Received 15 November 1999)

The performance of time-delayed feedback control is studied by linear stability analysis. Analytical approximations for the resulting eigenvalue spectrum are proposed. Our investigations demonstrate that eigenbranches that develop from the stable Lyapunov exponents of the free system also have a strong influence on the control properties, either by hybridization or by a crossing of branches which interchanges the role of the leading eigenvalue. Our findings are confirmed by numerical analysis of two particular examples, the Toda and the Rössler models. More important is the verification by actual electronic circuit experiments. Here, the observed reduction of control domains can be attributed to these additional eigenvalue branches. The investigations lead to a thorough analytical understanding of the stability properties in time-delayed feedback systems.

PACS number(s): 05.45.Gg

I. INTRODUCTION

Control of chaos has become an intense field of research within this decade, and therefore renewed interest in different control methods has been stimulated. In that context time-delayed feedback schemes have been rediscovered [1] since they are easy to apply in complex real world systems. Without performing complicated data analysis, the measurement of plain output signals is sufficient to generate online an appropriate control force from a time-delayed difference. The scheme applies to situations where one wants to stabilize formerly unstable temporal periodic states. Classical applications concern demonstrative experiments like mechanical oscillators [2] or electronic circuits [3], lasers [4], and discharge gas systems [5]. Meanwhile, the method has been used in quite diverse experimental contexts. We mention only spin wave dynamics beyond the Suhl instability, which even to date lacks adequate theoretical modeling, but time-delayed feedback control has been applied successfully [6].

Apart from this striking experimental success, an analytical understanding of the control method has been developed only recently. In that context it was pointed out that torsion, i.e., the finite imaginary part in the Floquet exponent, is a necessary ingredient for the method to work at all [7,8]. Furthermore, schemes for the adaptation of the delay time, which has to be adjusted to the period of the orbit, have been developed [9,10], and the limitations caused by the Lyapunov exponent of the orbit have been analyzed in detail [11]. Even the limiting influence of control loop latency, which is well known in the context of ordinary control theory, has been stressed for time-delayed feedback schemes [12]. Extensions of the simple scheme employing multiple delays [13], symmetry properties of the orbit under consideration [14], and time-dependent control amplitudes [15] have been discussed to overcome several of the limitations of the method just mentioned. Review articles dealing with several special aspects can be found in the literature (cf. [16]).

For theoretical analysis of the control performance one usually resorts to linear stability analysis or formally equivalent approaches. Hence the control properties are governed by the eigenvalue spectrum of the linearized equations of motion. Here we are going to deal with the structure of the whole spectrum, try to clarify how different eigenvalue branches interact with each other, and in particular demonstrate how branches that emerge from the stable exponents of the free system may influence the control properties. To keep the presentation self-contained and in order to set up the essential notation, we will first recall the main ideas of such theoretical approaches. Section III will be devoted to the study of eigenvalue spectra in different model equations using numerical simulations. It will become apparent that even low lying eigenvalue branches may considerably influence the control performance. These aspects are illustrated in electronic circuit experiments in Sec. IV. Several appendixes are concerned with technical details, which in principle are not new, but the application to time-delayed feedback control is sometimes difficult to find in the literature.

II. THEORETICAL ANALYSIS AND ANALYTICAL RESULTS

Time-delayed feedback schemes were invented for control of experimental systems where only a limited number of signals is accessible and no complicated data processing is possible. Typical examples are optical and magnetic experiments on ultrafast time scales or chemical and biological systems which are sensitive to environmental changes. A typical setup which covers all these cases is displayed in Fig. 1.

The equation of motion for the internal degrees of freedom which follows from the general setup reads

$$\dot{\boldsymbol{x}}(t)=\boldsymbol{f}(\boldsymbol{x}(t),KF(t)), \tag{1}$$

where the simplest recipe for the control force consists of a plain time-delayed difference of a single scalar signal,

*Electronic address: W.Just@qmw.ac.uk

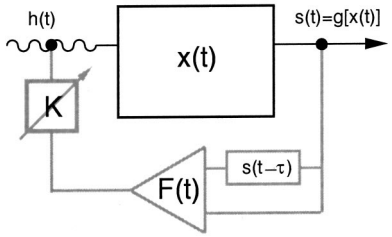

FIG. 1. Diagrammatic view of a time-delayed feedback control scheme. $\boldsymbol{x}(t)$ denotes the internal degrees of freedom of the nonlinear system, $s(t)$ the measured signal, and $h(t)$ external parameters or driving fields. The control loop is displayed in gray.

$$F(t)=g[\boldsymbol{x}(t)]-g[\boldsymbol{x}(t-\tau)]. \tag{2}$$

Such a scheme is suitable to control an unstable periodic orbit $\boldsymbol{\xi}(t)=\boldsymbol{\xi}(t+T)$ of the free system, $K=0$, provided the delay time τ is adjusted properly [1]. In what follows we choose $\tau=T$, so that the force finally vanishes when control is achieved.

The control performance is analyzed by considering the neighborhood of the periodic orbit and performing a linear stability analysis with the usual exponential ansatz,

$$\boldsymbol{x}(t)-\boldsymbol{\xi}(t)\simeq e^{(\Lambda+i\Omega)t}\boldsymbol{Q}(t), \quad \boldsymbol{Q}(t)=\boldsymbol{Q}(t+\tau). \tag{3}$$

Expanding the full equations of motion (1) and (2) one obtains an eigenvalue equation for the Floquet exponents $\Lambda+i\Omega$ and the eigenfunctions $\boldsymbol{Q}(t)$,

$$(\Lambda+i\Omega)\boldsymbol{Q}(t)+\dot{\boldsymbol{Q}}(t)=M[K(1-e^{-(\Lambda+i\Omega)\tau}),t]\boldsymbol{Q}(t). \tag{4}$$

Here the abbreviation on the right-hand side,[1]

$$M[\kappa,t]:=D_1\boldsymbol{f}(\boldsymbol{\xi}(t),0)+\kappa d_2\boldsymbol{f}(\boldsymbol{\xi}(t),0)\otimes Dg[\boldsymbol{\xi}(t)], \tag{5}$$

contains all the details of the internal dynamics and the coupling of the control force. Although we started from a differential-difference system we ended up with the usual Floquet-like problem (4). The price one has to pay is that the right hand side depends on the exponent itself. There exist fancy procedures for a numerical evaluation (cf. [17]), provided one has access to the explicit form of the equations of motion. But even without such information further simplification can be achieved. The matrix (5) itself has Floquet exponents [cf. Eq. (A1) for a formal definition] which depend on the argument κ. We will denote these quantities by $\Gamma^{(\nu)}[\kappa]$, where the superscript ν ranging between 1 and the dimension of the system (1) enumerates the different branches. Then Eq. (4) tells us that we recover the exponents of the controlled system if the correct value for the argument is inserted,

$$\Lambda+i\Omega=\Gamma^{(\nu)}[K(1-e^{-(\Lambda+i\Omega)\tau})]. \tag{6}$$

At the moment we do not know the function on the right hand side explicitly apart from the fact that its value at $\kappa=0$ reproduces the Floquet exponents of the free orbit,

[1] $D_k(d_k)$ denote the vector (scalar) derivatives with respect to the kth argument.

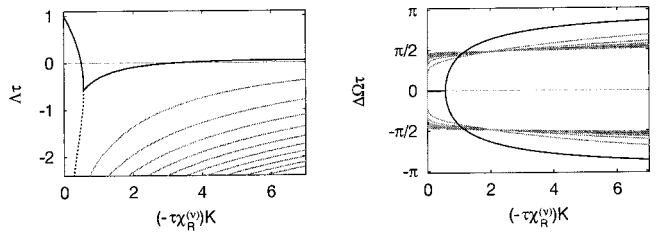

FIG. 2. Floquet exponents computed from Eq. (8) for $\lambda^{(\nu)}\tau=1$. Solid line: largest solution, dotted line: second real multiplier ($\Delta\Omega=0$), gray: nondominant complex exponents.

$$\Gamma^{(\nu)}[0]=\lambda^{(\nu)}+i\omega^{(\nu)}. \tag{7}$$

A simple but often quite useful approximation replaces $\Gamma^{(\nu)}[\kappa]$ by an affine function [cf. Eq. (A2)]. The reader may consult Appendix A, where several motivations for such a step are summarized.

In what follows we will concentrate on special types of free orbits, namely, those that flip their neighborhood during one turn. To be more definite we require that the Floquet multipliers are real so that the imaginary part of the Floquet exponent either vanishes or obeys $\omega^{(\nu)}=\pi/\tau$. In the latter case[2] the linear approximation just mentioned simplifies further and Eq. (6) reads in dimensionless units

$$\Lambda\tau+i\Delta\Omega\tau=\lambda^{(\nu)}\tau-(-\tau\chi_R^{(\nu)})K(1+e^{-\Lambda\tau-i\Delta\Omega\tau}). \tag{8}$$

Here $\Delta\Omega=\Omega-\pi/\tau$ denotes the deviation of the frequency due to control, and apart from the free Lyapunov exponent $\lambda^{(\nu)}\tau$ the only remaining system-dependent free parameter $(-\tau\chi_R^{(\nu)})$ captures all the details of the system. Of course, the latter coefficient may differ for the different Floquet branches of the matrix (5), but in each case it just rescales the control amplitude. The transcendental equation (8) can be discussed analytically (cf. Appendix B) and the final result for the Floquet exponents of the system subjected to control is shown in Fig. 2.

One branch emanating from the exponent of the free orbit collides at a critical control amplitude with a second real multiplier coming from minus infinity, and gives rise to a complex conjugated pair. For the real part of the largest exponent a typical butterfly shaped curve results, which eventually may lead to a finite control interval. There appears in addition an infinite number of complex valued Floquet exponents, which have smaller real parts and which tend to minus infinity in the limit of vanishing control amplitude. No crossing of the Floquet branches occurs within our analytical expression (8). An increase of the value of $\lambda^{(\nu)}\tau$ essentially shifts the whole set of curves upward.

The scenario displayed in Fig. 2 is generated by each of the Floquet exponents of the free system, which have been labeled by the superscript ν. The actual control domain is determined by the intersection of all these control intervals and a considerable reduction might result. Here we are par-

[2] If $\omega^{(\nu)}=0$ and $\lambda^{(\nu)}>0$ then, within the linear approximation, there always appears an eigenvalue with positive real part (cf. [8]). The same conclusion holds if the multiplier $\exp(\tau\Gamma^{(\nu)}[\kappa])$ is a real function.

ticularly interested in the question whether the branches originating from the initially stable exponents can influence the control performance. Such features cannot be successfully dealt with on the level of the linear approximation (8) since apart from other limitations such equations do not contain any coupling between different eigenspaces. Hence, we have to develop some improvement.

Expression (8) is an approximation for the full spectrum of the system under consideration. If one is interested in an improvement several constraints have to be observed. First of all, it is quite well known that the sum of all Floquet exponents is nothing else but the average of the trace of the matrix (5). Then

$$\sum_{\nu} \Gamma^{(\nu)}[\kappa] \overset{\text{mod } 2\pi i/\tau}{=} \frac{1}{\tau}\int_0^{\tau} \mathrm{Tr}\, D_1 \boldsymbol{f}(\boldsymbol{\xi}(t),0)dt + \kappa\frac{1}{\tau}\int_0^{\tau} Dg[\boldsymbol{\xi}(t)]d_2\boldsymbol{f}(\boldsymbol{\xi}(t),0)dt \tag{9}$$

implies that the sum of the exponents is strictly linear in κ. Hence

$$\Gamma^{(\nu)}[\kappa]=\lambda^{(\nu)}+i\omega^{(\nu)}+(\chi_R^{(\nu)}+i\chi_I^{(\nu)})\kappa+\Delta^{(\nu)}[\kappa], \qquad \sum_{\nu}\Delta^{(\nu)}[\kappa]=0, \tag{10}$$

is an exact expression, where $\Delta^{(\nu)}[\kappa]$ denotes the higher order nonlinear terms. It is already obvious from Eq. (4) that such correction terms are intimately related to the existence of different Floquet branches, since Eq. (8) becomes an exact expression for one-dimensional systems. As long as the control force is derived from a single scalar signal, at most one of the exponents increases linearly for large modulus $|\kappa|$ (cf. Appendix A) so that

$$\Delta^{(\nu)}[\kappa] \overset{|\kappa|\to\infty}{\simeq} -(\chi_R^{(\nu)}+i\chi_I^{(\nu)})\kappa \quad (\nu\neq\nu_{max}) \tag{11}$$

holds. Finally, the corrections $\Delta^{(\nu)}[\kappa]$ may be complex functions. However, like eigenvalues of matrices Floquet multipliers either are real or appear in complex conjugated pairs. The first possibility corresponds to an imaginary part of 0 or π/τ in the corresponding exponent whereas the second case implies frequencies that appear with opposite sign, e.g., $\omega^{(1)}=-\omega^{(2)}\neq 0,\pi/\tau$. If we specialize to free orbits with real multipliers, i.e., $\omega^{(\nu)}=0$ or π/τ, then, because of structural stability, the imaginary part does not change by small perturbation. Hence, a real first order coefficient results, $\chi_I^{(\nu)}=0$, and $\Delta^{(\nu)}[\kappa]$ is a real function at least for small argument. In summary, we stress that any improvement of Eq. (8) by nonlinear terms $\Delta^{(\nu)}[\kappa]$ has to obey the constraints just mentioned, but no simple extension containing only a few parameters is obvious at the moment.

III. MODELS AND NUMERICAL SIMULATIONS

We begin to test some of our theoretical results of the preceding section using numerical analysis of model systems. Such an approach might also help to improve simple analytical approximations like Eq. (8). There is of course an endless variety of models for performing numerical analysis. Here we concentrate on two simple but common systems, namely, the Toda and the Rössler equations. We employ a particular coupling of the control force and will fix most of the parameter values. We do not intend to give a complete overview of all control features of these models but focus on particular aspects of the stability problem.

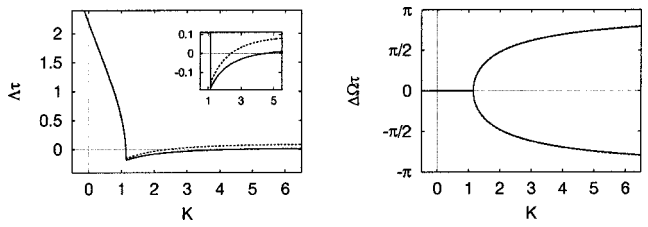

FIG. 3. Real part of the largest Floquet exponent and frequency deviation for the period-4 orbit of the Toda model (12) in dependence on the control amplitude (solid lines). The inset shows an enlargement of the control interval. Dotted lines display results according to the analytical expressions (13) and (6), but partly hidden since the coincidence is almost within the resolution of the figure.

A. Toda equation

The Toda oscillator represents a simple two-dimensional nonautonomous model system exhibiting chaos in certain parameter ranges. Its equations of motion read

$$\dot{x}_1=x_2, \qquad \dot{x}_2=-\mu x_2-\alpha(e^{x_1}-1)+A\sin(2\pi t)-K[x_2(t)-x_2(t-\tau)]. \tag{12}$$

Here the control term has already been included where the force was derived from the velocity coordinate. We will consider fixed parameter values $\mu=0.8$, $\alpha=25$, and study control properties for a few periodic orbits with integer periods.

As our first example let us consider the period-4 orbit at $A=84$. Floquet exponents are computed from the linearized equation of motion [cf. Eq. (4)] and the exponent with maximal real part is displayed in Fig. 3. One obtains the typical butterfly shaped curve for the real part already known from the simple analytical expression (8). In addition, lower and upper critical control amplitudes are observed, so that at least a qualitative agreement with the results of the preceding section is visible (cf. Fig. 2).

To check for quantitative coincidence we have calculated the exponents $\Gamma^{(1,2)}[\kappa]$ [cf. Eq. (A1)] and the result is shown in Fig. 4 for real values of the argument. In order to get an idea of which κ values are relevant for our spectrum, the figure displays also the location of the Floquet exponents $\Lambda+i\Omega$ in the complex κ plane according to the formula $\kappa=K[1-\exp(-\Lambda\tau-i\Omega\tau)]$.

A linear increase of one branch for large modulus is observed in accordance with the asymptotic behavior developed in Appendix A. The saturation of the other branch does not appear on the intermediate scale that is visible here. A pronounced hybridizationlike structure is visible near the origin. As a consequence a considerable curvature results and the linear approximation (A2) on which the analytical expression (8) was based is only correct to some limited extent. For a better quantitative agreement one has to take this struc-

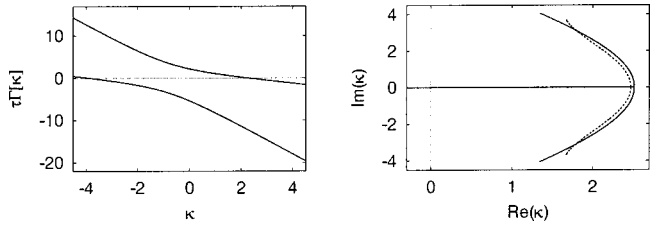

FIG. 4. Left: Dependence of the exponents $\tau\Gamma^{(1,2)}[\kappa]$ on real valued argument. Right: Location of the Floquet exponents (cf. Fig. 3) in the complex κ plane (solid line). Dotted lines are results from the analytical expression (13), but the coincidence is almost within the resolution of the figure.

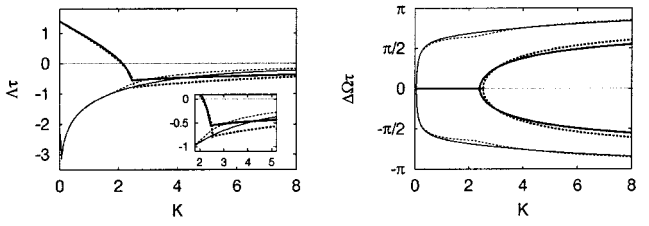

FIG. 5. Real part of two Floquet branches and frequency deviation for the period-1 orbit of the Toda model (12) in dependence on the control amplitude (solid lines). Thick (thin) line displays the branch connecting to the larger (smaller) Lyapunov exponent of the free system. Dotted lines display results according to the analytical expressions (13) and (6). The inset shows an enlargement near to the control threshold.

ture into account. In fact, one needs the full analytical structure of the expression $\Gamma^{(\nu)}[\kappa]$ in the complex plane, since even small deviations might result in spurious solutions of the eigenvalue equation. As an educated guess that has some heuristic theoretical support (cf. Appendix C) we suggest the expression

$$\tau\Gamma^{(1,2)}[\kappa]-i\pi=a+\alpha\kappa\pm(c+\gamma\kappa+\sqrt{b^2+\sigma\kappa+\beta^2\kappa^2}), \tag{13}$$

where the term within the parentheses may be considered as the nonlinear correction $\tau\Delta^{(1,2)}[\kappa]$. A fit to the data in Fig. 4 yields[3] $a=-1.6$ and $\alpha=-2$, which coincide of course with the exact analytical values according to the sum rule (9). The remaining parameters are obtained as $c=1.401$, $\gamma=0.000$, $b=2.385$, $\beta=1.381$, and $\sigma=3.046$. Here, deviations of the fit from the numerically obtained values of $\tau\Gamma^{(1/2)}[\kappa]$ are smaller than 0.5% and are not visible within the resolution of Fig. 4. In addition, the Floquet exponents of the controlled system, $\Lambda+i\Omega$, are also well reproduced (cf. Fig. 3). We stress that in the present case the lower eigenvalue influences the spectrum due to the hybridization just mentioned. However, no crossing of Floquet branches for the maximal exponent occurs.

The situation in the preceding paragraph seems to be less typical for the Toda model, since often a crossing of Floquet branches is observed. In order to demonstrate this feature we refer to the period-1 orbit at $A=105$. Floquet exponents in dependence on the control amplitude are displayed in Fig. 5.

One clearly recognizes that the branch emanating from the second stable exponent comes into play. Both branches display the well known frequency splitting transition but finally the former lower branch dominates the spectrum. This kind of behavior has already been observed for extended time-delayed feedback control [18], but no explanation has been given. Further, we note that in the case considered no upper critical control amplitude is obtained since the real part stays negative and the orbit remains linearly stable, at least for K values up to $K=20$. A fit for the analytical expression (13) yields $a=-0.4$, $\alpha=-0.5$, $c=0.4468$, $\gamma=0.0384$, $b=1.343$, $\beta=-3.176$, and $\sigma=0.000$. Again, the first two parameters coincide with their exact analytical values. The accuracy of the fit for $\Gamma^{(\nu)}[\kappa]$ is of the order of 5% and even the Floquet exponents are reasonably well reproduced (cf. Fig. 5).

[3]Fits to the data of $\Gamma^{(1)}[\kappa]+\Gamma^{(2)}[\kappa]$ and $\Gamma^{(1)}[\kappa]-\Gamma^{(2)}[\kappa]$ have been performed with GNUPLOT 3.7.

B. Rössler equation

As an example for an autonomous model we investigate the Rössler equation

$$\begin{aligned}\dot{x}_1&=-x_2-x_3-\varepsilon K[x_1-x_1(t-\tau)],\\ \dot{x}_2&=x_1+ax_2-K[x_2-x_2(t-\tau)],\\ \dot{x}_3&=b+x_1x_3-cx_3-\varepsilon K[x_3-x_3(t-\tau)],\end{aligned} \tag{14}$$

with parameter settings $a=0.82$, $b=0.55$, and $c=2.2$. For the coupling of the control force we have introduced a modified scheme which includes an additional parameter ε. For $\varepsilon=0$ conventional feedback control with a single scalar quantity is recovered. For $\varepsilon=1$ we obtain a coupling via the identity matrix. In such a case the simple expression (8) becomes exact (cf. Appendix A) and by changing the parameter ε deviations from the simple linear analytical approximation can be investigated systematically. As previously, a few branches of the Floquet spectrum for the period-1 orbit have been calculated numerically at different values of ε. They are shown in Fig. 6.

For $\varepsilon=1$, as already mentioned, the whole spectrum is described exactly by the simple analytical expression (8) (cf. Fig. 2). In order to understand which features change for $\varepsilon<1$, one has to concentrate on the real multipliers, which tend to minus infinity in the limit of vanishing control amplitude. For $\varepsilon<1$ these branches connect to each other, giving rise to a reversed third frequency splitting point that connects the formerly independent branches. On lowering ε further, two of the frequency splitting points collide at $\varepsilon\approx0.87$ giving rise to a cusp singularity. As a consequence the real and the complex branches become disconnected. The remaining frequency splitting point in the upper part of the spectrum is now caused by real branches that connect to the nontrivial Lyapunov exponents of the free system, in contrast to the situation at $\varepsilon=1$. Hence the branches originating from the uncontrolled exponents are no longer independent for $\varepsilon<0.87$ as Eq. (8) would imply. Therefore, the hybridization not only leads to quantitative deviations from the linear theory, but changes the structure of the spectrum completely,

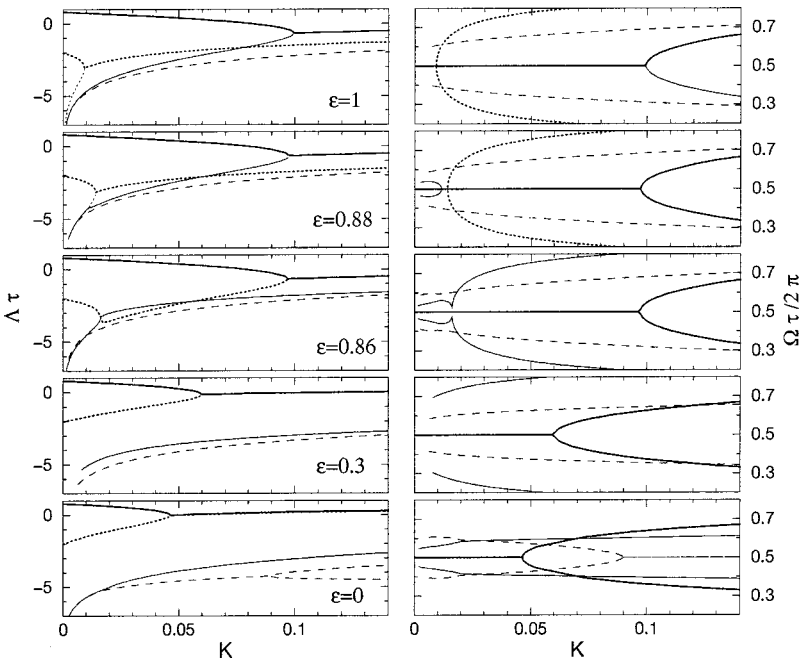

FIG. 6. Floquet exponents of the period-1 orbit of the Rössler system (14) in dependence on the control amplitude. Thick solid (dotted) line: branch originating from the free Lyapunov exponent $\lambda^{(1)}\tau=0.808(\lambda^{(3)}\tau=-2.026)$, dashed line: complex branch. The Goldstone mode connected to $\lambda^{(2)}\tau=0$ is not displayed.

so that the simple expression (8) no longer yields a good quantitative description. Nevertheless, the largest branch, which actually determines the stability of the orbit, preserves the typical butterfly shape.

To gain some more insight we have again calculated numerically the exponents $\Gamma^{(1,2,3)}(\kappa)$ for $\varepsilon=0$. The results are displayed in Fig. 7. The structure looks quite intricate, and in particular collisions of eigenvalues in the vicinity of $\kappa=0$ are observed. Since now three branches are involved, in contrast to the nonautonomous Toda equation, one cannot expect that expression (13) yields an overall quantitatively satisfactory description since the hybridization in Eq. (13) was based on two branches only. Although an extension to more branches is straightforward, it might become meaningless since the number of free parameters increases. Nevertheless, the linear increase of $\Gamma^{(3)}[\kappa]$ and the saturation of $\Gamma^{(1,2)}[\kappa]$ are again in accordance with the general considerations of Appendix A.

The complexity of the studied case of the Rössler system indicates that the fine structure of the Floquet spectrum in higher dimensional systems is in general quite complicated and difficult to describe quantitatively by analytical methods. Surely such complicated spectra may also be detected in different models. One can conclude that the type of spectrum depends strongly on the specific properties of the system and the coupling of the control. However, the main features are well captured qualitatively even by simple expressions like Eq. (8).

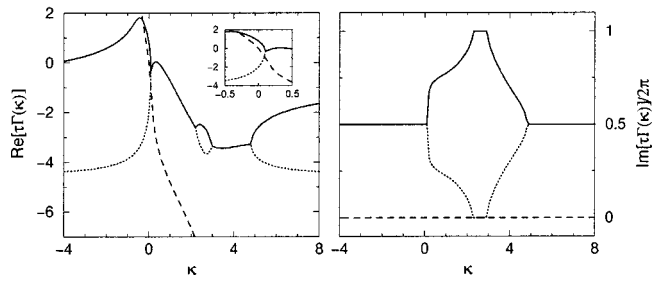

FIG. 7. Dependence of the exponents $\tau\Gamma^{(1,2,3)}[\kappa]$ on real valued argument for the period-1 orbit of the Rössler system for $\varepsilon=0$. $\tau\Gamma^{(1)}[\kappa]$ (solid) connects to the free exponent $\lambda^{(1)}\tau=0.808$, $\tau\Gamma^{(3)}[\kappa]$ (dotted) to $\lambda^{(3)}\tau=-2.026$, and $\tau\Gamma^{(2)}[\kappa]$ (dashed) to the Goldstone mode with $\lambda^{(2)}\tau=0$. The inset shows the bifurcation structure close to $\kappa=0$.

IV. ELECTRONIC CIRCUIT EXPERIMENTS

So far our investigations have shown that the principal aspects of the Floquet spectrum are well understood. Even the simple theory captures basic features of the control performance and deviations can be attributed to nonlinear contributions of the characteristic equation (6). One can even model these terms successfully in special cases. Hence, it seems promising to continue our investigations with real experimental systems.

In almost all our experiments on chaos control by time-delayed feedback we have observed the existence of several Floquet exponents, at least for high control amplitude. In most cases the control regime was determined solely by the branch that connects to the unstable free Lyapunov exponent. A second or even several exponents appear in the spectrum of the control signal for high K values but often do not cross the first one. In a few cases, such a crossing appeared in the real parts, leading to a reduced control domain. Here we report on these phenomena in experiments on a nonlinear diode resonator. The circuit (cf. Fig. 8), consisting of a diode (1N4005), an inductor L, and a resistor R, was sinusoidally driven at fixed frequency f_A with amplitude U_A. The control device allows application of a control force of the form $F(t)=K[U(t)-U(t-\tau)]$, where the delay was set according to the driving frequency. Our feedback scheme consisted of coupling the voltage at the resistor via the control device to the driving force.

A. Quasilinear behavior of Floquet spectra

Our first set of parameters $L=760$ μH, $R=36$ Ω, $f_A=800$ kHz, and $U_A=1.1$ V guaranteed a chaotic attractor

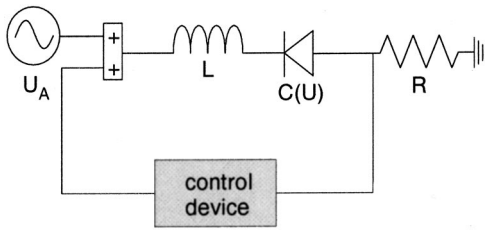

FIG. 8. Experimental setup of the nonlinear diode resonator with control device.

that emerged from a period-doubling cascade on variation of the driving amplitude. Above all, this sequence of bifurcations left behind an unstable period-1 orbit with frequency $\omega=\pi/T$ in the Floquet exponent, which was generated in the first period-doubling bifurcation. Applying time-delayed feedback it is possible to stabilize this orbit for control amplitudes K between 12.9 and 81.7. We want to demonstrate how the Floquet exponent with the largest real part, determining the stability of the orbit, changes on variation of the control amplitude.

There are several possibilities to determine Floquet exponents of a periodic orbit from experiment. One would be to stabilize the orbit by time-delayed feedback and apply an additional small harmonic force. By sweeping its frequency and measuring the response of the system at every particular frequency point, one obtains the power spectrum of the linear response function. Although its detailed form is in general quite complicated, the least stable eigenvalues are signaled by Lorentzian lines (cf. Appendix D). The corresponding spectra that have been measured in the control interval are displayed in Fig. 9.

From the position and width of the lines it is possible to determine the Floquet exponents [cf. Eq. (D10)]. In particular, the dominant line gives the Floquet exponent with largest real part (cf. Fig. 10). For comparison with the analytical result (8) we optimized the fit with respect to the frequency splitting point, obtaining $\lambda\tau=1.07$ and $(-\tau\chi_R)=0.036$. The quantitative coincidence with this linear model is within a few percent. At first glance one does not observe several Floquet branches in the spectra (cf. Fig. 9), but realizes strange non-Lorentzian peak forms for high control amplitude. On a closer look, this can be attributed to the existence of several lines within a small frequency band (cf. Fig. 11).

Unfortunately it is not possible to extract these additional Floquet branches for a wider K range from these measurements, especially since the number of ''visible'' exponents increases with the applied control amplitude. Therefore, only the exponent with largest real part is plotted in Fig. 10. To conclude, this is one experimental example where several Floquet exponents appear in the spectrum of the control signal for high K values but do not cross the first one. Here, the stability of the controlled orbit is solely determined by the exponent that connects to the unstable free Lyapunov exponent.

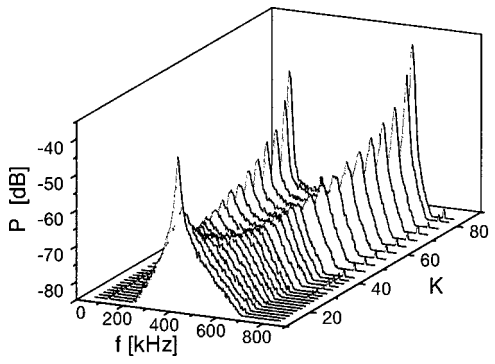

FIG. 9. Network analyzer spectra of the control signal for the stabilized but disturbed orbit.

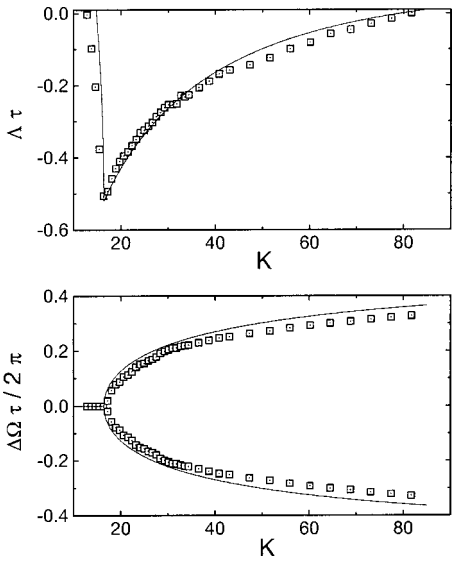

FIG. 10. Floquet branch with largest real part for the period-1 orbit of the nonlinear diode resonator in dependence on the control amplitude. Solid lines display fits according to the analytical result (8) with $\lambda\tau=1.07$ and $(-\tau\chi_R)=0.036$.

B. Reduced control domains due to Floquet branch crossing

As a second example we used $L=517$ μH, $R=124\,\Omega$, and $f_A=813$ kHz. Although the method described above works quite accurately within the control interval, it does not allow Floquet exponents to be obtained outside the stability domain. Therefore, in contrast to the former experiments, here we utilized a different method for extracting the Floquet exponents of the system. We determined the real part by analyzing the exponential decrease (increase) from transients

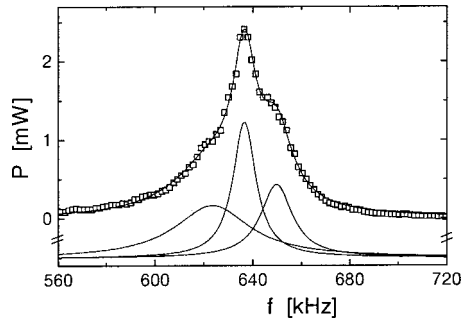

FIG. 11. Extended view of the network analyzer spectrum for $K=60$ (cf. Fig. 9). In addition to the experimental data, a fit with three Lorentzian lines (for clarity moved downward) and their sum is depicted.

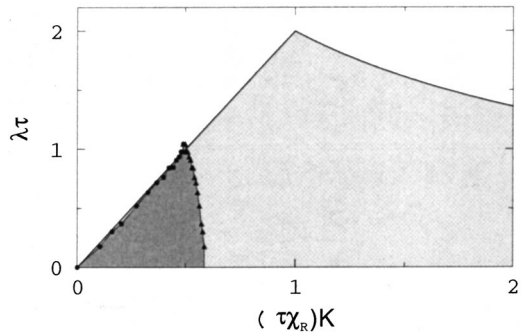

FIG. 12. Control domain for the diode resonator in the plane of control amplitude and free Lyapunov exponent: circles, lower threshold (flip bifurcation); triangles, upper threshold (Hopf bifurcation). Solid line and light gray shaded region correspond to the analytical result Eq. (8) with $(-\tau\chi_R)=0.088$.

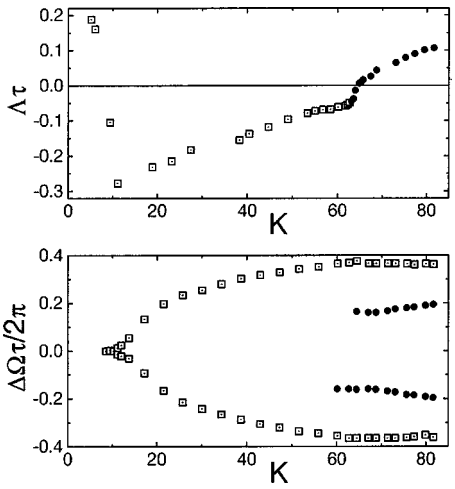

FIG. 13. Floquet branch with largest real part and frequency deviation for the period-1 orbit of the nonlinear diode resonator in dependence on the control amplitude: open symbols, branch connecting to the free unstable Lyapunov exponent; full symbols, crossing complex branch.

of the control signal when switching the control on (to a K value outside the control interval). The imaginary part was obtained from the frequency spectrum of this transient. Such a procedure allows the Floquet exponents to be determined in the whole K range, in particular, the Lyapunov exponent of the free orbit, λ, for $K=0$. By changing the driving amplitude U_A between 0.7 and 3.2 V unstable period-1 orbits with different positive free Lyapunov exponents could be realized. Sweeping the control amplitude K, we obtained the lower and the upper border of the control interval (cf. Fig. 12).

We have compared this control domain with the analytical prediction according to Eq. (8) (cf. [11]). Here the fit of the lower control threshold can be achieved with a single value of the scaling parameter $(-\tau\chi_R)$, which indicates that the dependence of this quantity on the system parameters in the parameter interval under consideration is very weak. For the upper control threshold a considerable reduction of the control domain is observed and control is no longer possible for $\lambda\tau>1.1$, in contrast to the predictions of the linear expression (8). Along the left border of the domain the frequency attains a constant value, $\Delta\Omega=0$, whereas on the right border it varies continuously. Since at the tip of the region the frequency develops a finite jump, we conclude that the cutoff of the region is caused by a different Floquet branch.

We demonstrate this phenomenon by Floquet spectra obtained at parameter values $L=470$ μH, $R=127$ Ω, $f_A=813$ kHz, and $U_A=1$ V. As can be seen clearly from our experimental results (cf. Fig. 13), the control interval is not determined only by the first Floquet exponent. A crossing in the real part occurs, leading to a new dominant Floquet branch. As a consequence a considerable reduction of the control interval takes place.

V. CONCLUSION

Linear stability analysis is a useful tool to study the performance of time-delayed feedback control. The corresponding characteristic equation can be written down formally and may be solved by numerical methods if the equations of motion are known. But analytical evaluation calls for some approximation. The simplest version, i.e., Eq. (8), already captures essential qualitative features, e.g., the bifurcations that limit the control interval. However, such an expression does not contain all properties of the spectrum. In particular, the interaction of different eigenvalue branches, which originate from different exponents of the free system, is not properly taken into account, so that at least quantitative deviations occur.

The influence of these additional branches, which are stable in the free system, is twofold. On the one hand, hybridization between the different branches may occur so that the right hand side of the characteristic equation (6) deviates considerably from the linear form that has been employed in the approximation (8). A more complicated expression has been adopted [cf. Eq. (13)], which yields good quantitative coincidence with numerical simulations of the Toda equation. The price one has to pay is an increase of the number of free parameters that have to be fitted to numerical data. On the other hand, eigenvalue branches may cross and the eigenvalue with largest real part, which determines the stability, may change. Then, the branch that originates from the stable exponent of the free system may enter the business, as exemplified by the numerical study of the Toda equation. In particular, such crossings have been identified in the electronic circuit experiment. As a consequence a considerable reduction in the control domain and a reduction of accessible periodic orbits results.

The simple analytical expression (8) becomes exact for a mean field type coupling of the control force. With the investigation of the Rössler system we have studied systematically deviations from such a situation. Finally, the different eigenvalue branches become intermingled in a cusp point, and the whole structure of the spectrum changes qualitatively if the case of the original Pyragas scheme is considered.

So far we have seen that the linear stability properties of time-delayed feedback control can be modeled even on analytical grounds to a certain extent. For a full understanding of the control performance, there are, however, several aspects left, and we mention three of them which in our opinion are the major challenge for future research. First, we have already seen on analytical as well as on numerical grounds that for large control amplitudes the real part of the Floquet ex-

ponents tends toward zero, i.e., exponents accumulate at the stability threshold. Even if the real part stays negative so that the orbit is formally stable, small perturbations, e.g., noise may render the orbit unstable and strongly influence the upper critical control threshold. In particular, in experimental systems such a weak stability of the orbit can be destroyed by the presence of imperfections. Hence, it is of utmost importance to study the stability of the spectrum against perturbations, a problem that plays a major role in the context of strongly non-normal operators.

Second, there exists at least one variant of the control algorithm which we believe deserves a closer look. Our investigations indicate that the number of measured signals from which control forces are derived plays a major role in the structure of the eigenvalue problem and hence in the control performance. If several quantities are employed to derive control forces, not only do different control amplitudes enter the business but there appears a wider range of possibilities to couple these forces to the system under consideration. Hence, one may look for some optimized coupling scheme, a problem that is well established in the context of control theory. However, to the best of our knowledge only preliminary results exist for time-delayed feedback control of periodic states (cf. [17]).

Third, the domain of attraction of the stabilized orbit plays a major role in applications. Surely such a property is beyond the linear stability analysis, and even in ordinary differential equations the estimation of the domain of attraction is among the most difficult tasks. Thus, one might expect that the corresponding problem in time-delay systems will be even harder to tackle. However, the size of the domain of attraction is expected to be of equal importance with the stability itself.

ACKNOWLEDGMENTS

Main parts of the work have been performed during a stay (W.J.) at the Max-Planck-Institute for Fluid Dynamics, Göttingen, Germany. We are indebted to F. Laeri and M. Müller for the use of their delayed feedback control device. Part of this work was supported by Deutsche Forschungsgemeinschaft through SFB 185 ''Nichtlineare Dynamik.'' P.F. acknowledges financial support from the SOCRATES program of the European Community.

APPENDIX A: ASYMPTOTIC EXPANSION OF THE CHARACTERISTIC EQUATION

In order to evaluate the characteristic equation (6) explicitly one needs an expression for the Floquet exponents of the matrix (5). The latter are defined by the eigenvalue problem

$$\Gamma^{(\nu)}[\kappa]\boldsymbol{P}_\kappa^{(\nu)}(t)+\dot{\boldsymbol{P}}_\kappa^{(\nu)}(t)=M[\kappa,t]\boldsymbol{P}_\kappa^{(\nu)}(t),$$
$$\boldsymbol{P}_\kappa^{(\nu)}(t)=\boldsymbol{P}_\kappa^{(\nu)}(t+\tau), \tag{A1}$$

where $\boldsymbol{P}_\kappa^{(\nu)}$ denotes the corresponding right eigenfunctions. We have already stressed in the main text that a useful approximation is given by an affine expression,

$$\Gamma^{(\nu)}[\kappa]=\lambda^{(\nu)}+i\omega^{(\nu)}+(\chi_R^{(\nu)}+i\chi_I^{(\nu)})\kappa. \tag{A2}$$

Here the constant term is just the Floquet exponent of the free system by virtue of Eqs. (5) and (A1).

The validity of Eq. (A2) is not obvious and calls for several comments. The simplest argument consists in a Taylor series expansion. If we choose some arbitrary base point κ_0 and neglect all contributions of second and higher order, we obtain

$$\Gamma^{(\nu)}[\kappa]=\Gamma^{(\nu)}[\kappa_0]-\frac{d\Gamma^{(\nu)}}{d\kappa_0}\kappa_0+\frac{d\Gamma^{(\nu)}}{d\kappa_0}\kappa+O[(\kappa-\kappa_0)^2]. \tag{A3}$$

The constant term yields at least an estimate for the free Floquet exponent [cf. Eq. (7)] and Eq. (A2) constitutes a locally correct asymptotic expression.

Nevertheless, one may consider under what conditions higher order terms can be neglected. We will show that Eq. (A2) becomes exact for a particular type of coupling of the control force. Suppose that we can replace the control matrix, i.e., the second term in the definition (5) by a multiple of the unity matrix, $\alpha\mathbf{1}$. Such a situation happens if one couples each component of the state vector to one of the equations of motion in a diagonal way with strength α (cf. [6]). Such a coupling may be called mean field like. Then the eigenvalue problem (A1) simplifies to

$$[\Gamma^{(\nu)}[\kappa]-\alpha\kappa]\boldsymbol{P}_\kappa^{(\nu)}(t)+\dot{\boldsymbol{P}}_\kappa^{(\nu)}(t)=D_1\boldsymbol{f}(\boldsymbol{\xi}(t),0)\boldsymbol{P}_\kappa^{(\nu)}(t), \tag{A4}$$

taking the definition (5) into account. But Eq. (A4) tells us that $\Gamma^{(\nu)}[\kappa]-\alpha\kappa$ coincides with the Floquet exponent of the free system and expression (A2) is recovered with $\chi_R^{(\nu)}=\alpha$ and $\chi_I^{(\nu)}=0$.

Finally, we emphasize that in the general case a linear dependence is obtained for large values of $|\kappa|$ also. Such a feature may already be guessed from the linear dependence of the matrix (5) on κ. This rough argument can be based on a formal perturbation expansion. If we confine ourselves to the case that the control force is derived from a single scalar quantity [cf. Eq. (2)] then the dominant term in Eq. (5) is a dyadic product. As a consequence there appear two different kinds of eigenbranches $\Gamma^{(\nu)}[\kappa]$. One branch, labeled by ν_{max} for convenience, admits an eigenfunction proportional to $d_2\boldsymbol{f}$ such that

$$\Gamma^{(\nu_{max})}[\kappa]=\kappa\gamma_1+O(\kappa^0),$$
$$\boldsymbol{P}_\kappa^{(\nu_{max})}(t)=e^{\kappa a_1(t)+O(\kappa^0)}[d_2\boldsymbol{f}(\boldsymbol{\xi}(t),0)+O(\kappa^{-1})]. \tag{A5}$$

All other eigenfunctions are orthogonal to Dg and the corresponding Floquet exponent does not possess a contribution in leading order,

$$\Gamma^{(\nu)}[\kappa]=O(\kappa^0),$$
$$Dg[\boldsymbol{\xi}(t)]\boldsymbol{P}_\kappa^{(\nu)}(t)=O(\kappa^{-1})\quad(\nu\neq\nu_{max}). \tag{A6}$$

The computation of these expansions is standard, but here we focus on the dominant branch (A5) only. Inserting Eq. (A5) into Eq. (A1), we obtain in order $O(\kappa)$, taking the definition (5) into account,

$$[\gamma_1+\dot{a}_1(t)]d_2\boldsymbol{f}(\boldsymbol{\xi}(t),0)=d_2\boldsymbol{f}(\boldsymbol{\xi}(t),0)\{Dg[\boldsymbol{\xi}(t)]d_2\boldsymbol{f}(\boldsymbol{\xi}(t),0)\}. \tag{A7}$$

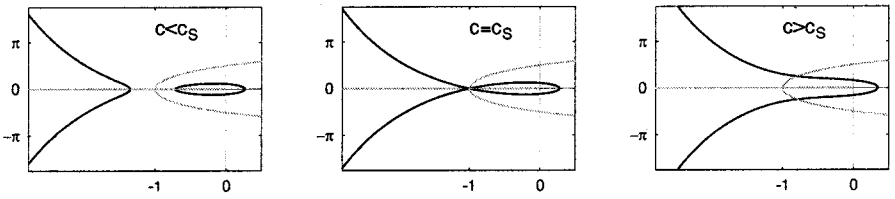

FIG. 14. Solution curves of Eq. (B3) (solid lines) in the complex z plane for $c<c_S$, $c=c_S$, and $c>c_S$ (from left to right). For comparison the solution of Eq. (B4) is also shown (gray lines).

Since $a_1(t)$ is periodic, plain integration leads to

$$\gamma_1=\frac{1}{\tau}\int_0^\tau Dg[\boldsymbol{\xi}(t)]d_2\boldsymbol{f}(\boldsymbol{\xi}(t),0)dt. \tag{A8}$$

The asserted linear dependence is obtained from Eq. (A5) in leading order if the coefficient (A8) does not vanish. It is remarkable that such a condition is violated if, e.g., the control force couples only a single component of the state vector to a single equation in a nondiagonal manner, since the scalar product in Eq. (A8) will vanish. Our analysis might indicate why such coupling schemes are often not very effective.

In summary, our arguments indicate why such a rough approximation as Eq. (A2) may work well in a general context. It is also clear that inclusion of higher order terms should not violate the linear asymptotics for large κ. Furthermore, one should not confuse the large κ asymptotics with the limit of large control amplitudes, since the argument in the characteristic equation (6) contains the Floquet exponent also. In fact, a closer inspection of the approximation (8) reveals that the argument $K[1+\exp(-\Lambda\tau-i\Delta\Omega\tau)]$ may saturate at a finite value for large control amplitudes, since the second factor tends to zero. However, and above all, we want to stress that the linear approximation (A2) makes sense only for the Floquet exponents but not for the multipliers. The latter involve an exponential dependence on κ, and approximations along the lines of a plain series expansion would be completely useless.

APPENDIX B: SOLUTION OF THE TRANSCENDENTAL CHARACTERISTIC EQUATION

The analytical investigation of Eq. (8) is to some extent standard and essential parts can be found in textbooks (cf. [19]). Nevertheless, we present here an explicit and elementary discussion for completeness. First of all, the following abbreviations for the eigenvalues and the control amplitude are introduced:

$$\begin{aligned} z &:= \Lambda\tau+i\Delta\Omega\tau-\lambda\tau+(-\tau\chi_R^{(\nu)})K, \\ c &:= (-\tau\chi_R^{(\nu)})Ke^{-\lambda\tau+(-\tau\chi_R^{(\nu)})K}. \end{aligned} \tag{B1}$$

Then Eq. (8) simplifies to

$$z=-ce^{-z}. \tag{B2}$$

While z may in general be a complex valued quantity, c denotes a real number. Its sign corresponds to the sign of the control amplitude.

The real valued solutions of Eq. (B2) are computed fairly easily. One just has to intersect an exponential with a straight line. For $c<0$ a single solution exists, since the left hand side of Eq. (B2) is linearly increasing and the right hand side exponentially decaying. For $0<c<c_S:=1/e$, two solutions are present, where the smaller one tends to minus infinity as c approaches zero. At c_S both solutions collide and no real solution exists any more for larger c values. Solving Eq. (B2) for c yields the properties just described in a c-Re(z) diagram (cf. Fig. 2).

For the discussion of complex solutions we confine ourselves to the case $c>0$, i.e., $(-\tau\chi_R^{(\nu)})K>0$, for simplicity. The other possibility ($c<0$) does not include new features since the real solution mentioned above already indicates instability. In polar coordinates $z=r\exp(i\varphi)$, Eq. (B2) reads

$$r=ce^{-r\cos\varphi}, \tag{B3}$$

$$\varphi=\pi-r\sin\varphi, \tag{B4}$$

where for the angle φ we allow any real value. Each equation describes a set of curves in the complex plane and its intersection points yield the desired eigenvalues.

The curves determined by Eq. (B3) and their dependence on c are summarized in Fig. 14. As for the analytical computation of this diagram, we recall that Eq. (B3) is of the just discussed type that involves a linear and an exponential term, provided we are looking for r in terms of φ. Depending on the sign of $\cos\varphi$, either one or two solutions may exist. For $\varphi\in(-\pi/2,\pi/2)|\mathrm{mod}\,2\pi$, $\cos\varphi>0$ holds and exactly one solution $r=r(\varphi)$ exists. That branch gives rise to the loop in the region $\mathrm{Re}(z)>0$. For $\varphi\in(\pi/2,3\pi/2)|\mathrm{mod}\,2\pi$ two cases have to be distinguished. If $0<c<c_S$ holds, one always obtains two solutions, which depend monotonically on $\cos\varphi$. This case completes the leftmost diagram in Fig. 14. At $c=c_S$ a critical case happens, since the two solutions of Eq. (B3) just touch at $r=1$, $\varphi=\pi$. As a consequence the two disconnected parts of the curve join. For $c>c_S$, Eq. (B3) has two real solutions only if $\cos\varphi$ is not too small, i.e., $\cos\varphi>\cos\varphi_0(<0)$. The actual value of the critical angle φ_0 does not matter, but it is easily computed from the condition that the two solutions collide. The monotonic dependence of the solutions on $\cos\varphi$ together with the fact that one of the real solutions tends to infinity in the limit $\cos\varphi\uparrow 0$ yields the rightmost diagram in Fig. 14. A parametric representation of all these curves may be obtained by solving Eq. (B3) for $\cos\varphi$. In particular, the asymptotic representation $\mathrm{Im}(z)\simeq\pm c\exp[-\mathrm{Re}(z)]$ follows in the limit $\mathrm{Re}(z)\to-\infty$, so that the curves increase exponentially to the left.

The curves determined by Eq. (B4) do not depend on the value of c and are depicted in Fig. 15. As for the analytical computation we first note the trivial solution $\varphi=\pi$, $r\geqslant 0$. Furthermore, it would be sufficient to consider the upper half plane $\varphi\in(0,\pi)|\mathrm{mod}\,2\pi$ since Eq. (B4) is invariant with

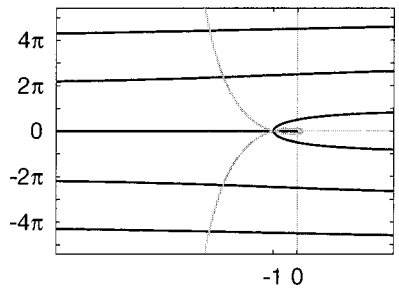

FIG. 15. Solution curves of Eq. (B4) (solid lines) in the complex z plane. For comparison the solution of Eq. (B3) for $c=c_S$ is also shown (gray lines). The actual value of c does not influence the large scale properties of the latter curve.

respect to the substitution $\pi-\varphi\rightarrow\varphi-\pi$, and the curves are symmetric with respect to the horizontal axis. Since according to Eq. (B4)

$$r=\frac{\pi-\varphi}{\sin\varphi} \tag{B5}$$

holds and r is non-negative, only a restricted set of angles is possible, namely, $\varphi\in I_n$, where $I_0=[0,2\pi]$, $I_{n\geqslant 1}=[(2n+1)\pi,(2n+2)\pi]$, and $I_{n\leqslant -1}=[2n\pi,(2n+1)\pi]$. Equation (B4) just tells us that in each interval I_n the imaginary part $r\sin\varphi$ changes monotonically. For $n\neq 0$ this yields the branches in Fig. 15 that do not touch the horizontal axis. For $n=0$ Eq. (B4) implies the limits $r=1$ at $\varphi=\pi$, and $r=\infty$ at $\varphi=0$, so that the forklike structure depicted in Fig. 15 follows.

The intersection of the two graphs yields the desired eigenvalues (cf. Figs. 14 and 15). The shape of the curve in Fig. 14 and the inequality $c_S\ll\pi$ guarantee that the solution with largest real part is either one of the real solutions or the complex solution that occurs on the collision of the two reals. A crossing of eigenvalue branches does not occur. The analysis of other cases, e.g., $c<0$ or even complex free Floquet multipliers $\omega^{(\nu)}\neq 0,\pi$, follows the same lines. In particular, parts of the analysis do not change since c enters only Eq. (B3) and a finite imaginary part would influence only Fig. 15.

We admit that additional and sometimes tedious analytical estimates are necessary to prove rigorously all topological features of Figs. 14 and 15. But the steps that the mathematically intended reader might feel to be missing can be supplemented. They have been skipped here for clarity and brevity. In addition, one should keep in mind that the results just mentioned can be obtained by more abstract approaches also (cf. [20]).

APPENDIX C: HYBRIDIZATION OF FLOQUET BRANCHES

The Floquet exponents $\Gamma^{(\nu)}[\kappa]$ [cf. Eq. (A1)] are usually computed with the help of the evolution matrix

$$\dot{\mathbf{U}}_\kappa(t)=M[\kappa,t]\mathbf{U}_\kappa(t),\quad \mathbf{U}_\kappa(0)=\mathbf{1}. \tag{C1}$$

The exponents are just the logarithms of the eigenvalues of $\mathbf{U}_\kappa(\tau)$. Floquet theory tells us that the evolution matrix splits into a periodic and an exponentially time-dependent factor. For $\kappa=0$ this splitting reads

$$\mathbf{U}_0(t)=\mathbf{Q}_0(t)\exp(\mathbf{C}_0 t),\quad \mathbf{Q}_0(t)=\mathbf{Q}_0(t+\tau), \tag{C2}$$

where $\mathbf{C}_0$ determines the free Floquet exponents. The splitting (C2) is, of course, not unique and different rules for the imaginary part result in different periodic factors $\mathbf{Q}_0(t)$. We use a periodic factor to simplify Eq. (C1). Introducing

$$\mathbf{V}_\kappa(t)=\mathbf{Q}_0^{-1}(t)\mathbf{U}_\kappa(t), \tag{C3}$$

we obtain

$$\dot{\mathbf{V}}_\kappa(t)=[\mathbf{C}_0+\kappa\boldsymbol{\alpha}(t)\otimes\boldsymbol{\beta}(t)]\mathbf{V}_\kappa(t), \tag{C4}$$

where the vectors in the control matrix are given by

$$\boldsymbol{\alpha}(t)\otimes\boldsymbol{\beta}(t)=\mathbf{Q}_0^{-1}(t)d_2\mathbf{f}(\boldsymbol{\xi}(t),0)\otimes Dg[\boldsymbol{\xi}(t)]\mathbf{Q}_0(t). \tag{C5}$$

Floquet exponents can be obtained from the matrix (C3) because of initial and periodicity conditions. In order to solve Eq. (C4) analytically we introduce a crude approximation and neglect completely the time dependence of the vectors (C5). We have to mention that this approximation is not invariant with respect to the convention for the imaginary part of the Floquet exponents since different periodic factors $\mathbf{Q}_0(t)$ imply different constraints for the control vectors. Furthermore, the matrix $\mathbf{Q}_0(t)$ may be complex valued, a case that appears in particular if all multipliers of the free system are negative, i.e., $\omega^{(\nu)}=\pi/\tau$. However, in the case on which we concentrate in what follows, the factor $\exp(-i\pi t/\tau)$ may be absorbed in the definition of $\mathbf{Q}_0(t)$, which then becomes a real but antiperiodic quantity. Fortunately, Eq. (C5) stays periodic in time and the assumption of constant vectors remains consistent.

Hence, we are left with the diagonalization of the matrix $\mathbf{C}_0+\kappa\boldsymbol{\alpha}\otimes\boldsymbol{\beta}$, where the first term has eigenvalues $\lambda^{(\nu)}$. If we restrict ourselves to the two-dimensional case the desired Floquet exponents read

$$\tau\Gamma^{(1,2)}[\kappa]-i\pi=\tfrac{1}{2}(\lambda^{(1)}+\lambda^{(2)}+\kappa\langle\boldsymbol{\beta}|\boldsymbol{\alpha}\rangle)\pm\sqrt{\tfrac{1}{4}(\lambda^{(1)}-\lambda^{(2)})^2+\tfrac{1}{2}(\lambda^{(1)}-\lambda^{(2)})(\alpha_1\beta_1-\alpha_2\beta_2)\kappa+\tfrac{1}{4}\langle\boldsymbol{\beta}|\boldsymbol{\alpha}\rangle^2\kappa^2}. \tag{C6}$$

Expression (C6) has, of course, the correct asymptotic behavior for large values of $|\kappa|$ as described in Appendix A. For our purpose we need the branches in an intermediate κ range and expression (C6) is not fully sufficient. In order to keep all coefficients independent of each other we generalize to Eq. (13), which is the most general expression having linear asymptotic behavior and involving square root singularities only. It takes the hybridization of the two branches into account appropriately.

APPENDIX D: LINEAR RESPONSE FOR DELAY SYSTEMS

Consider a system subjected to time-delayed feedback control and an additional small time-dependent external parameter $b(t)$,

$$\dot{\boldsymbol{x}}(t)=\boldsymbol{F}(\boldsymbol{x}(t),KF(t),b(t)). \tag{D1}$$

In the vicinity of the periodic orbit $\boldsymbol{\xi}(t)$ the dynamics up to first order is given by

$$\begin{aligned}\delta\dot{\boldsymbol{x}}(t)=&D_1\boldsymbol{f}(\boldsymbol{\xi}(t),0)\delta\boldsymbol{x}(t)+d_2\boldsymbol{f}(\boldsymbol{\xi}(t),0)\{Dg[\boldsymbol{\xi}(t)]\\&\times K[\delta\boldsymbol{x}(t)-\delta\boldsymbol{x}(t-\tau)]\}+d_3\boldsymbol{F}(\boldsymbol{\xi}(t),0,0)b(t),\end{aligned} \tag{D2}$$

where in accordance with Sec. II the notation $\boldsymbol{F}(\boldsymbol{x},F,0)=\boldsymbol{f}(\boldsymbol{x},F)$ was used. Provided the periodic orbit subjected to control is stable, Eq. (D2) governs the whole dynamics in its vicinity for small driving fields. Because of linearity the solution of Eq. (D2) may be obtained for each Fourier mode of the field $b(t)$ separately, $b_w\exp(iwt)$. The corresponding mode of the response $\delta\boldsymbol{x}(t)$ after discarding a transient is given by $\mathbf{r}_w(t)\exp(iwt)$ with $\mathbf{r}_w(t)=\mathbf{r}_w(t+\tau)$. By virtue of Eq. (D2) it obeys

$$\frac{d}{dt}[\mathbf{r}_w(t)e^{iwt}]=M[\mu_w,t]\mathbf{r}_w(t)e^{iwt}+d_3\boldsymbol{F}(\boldsymbol{\xi}(t),0,0)b_we^{iwt},$$

$$\mu_w:=K(1-e^{-iw\tau}), \tag{D3}$$

where the abbreviation (5) has been used. The solution of this linear inhomogeneous equation in the stationary state may be obtained by employing the evolution matrix (C1). By the usual spectral decomposition the latter can be expressed in terms of right and left eigenfunctions which are defined by Eq. (A1) and

$$\begin{aligned}\Gamma^{(\nu)}[\kappa]\boldsymbol{p}_\kappa^{(\nu)*}(t)-\dot{\boldsymbol{p}}_\kappa^{(\nu)*}(t)&=\boldsymbol{p}_\kappa^{(\nu)*}(t)M[\kappa,t],\\ \boldsymbol{p}_\kappa^{(\nu)}(t)&=\boldsymbol{p}_\kappa^{(\nu)}(t+\tau).\end{aligned} \tag{D4}$$

Then the stationary solution of Eq. (D3) reads

$$\begin{aligned}\mathbf{r}_w(t)e^{iwt}=&\int_{-\infty}^{t}\sum_\nu e^{\Gamma^{(\nu)}[\mu_w](t-t')}\\&\times\frac{\mathbf{P}_{\mu_w}^{(\nu)}(t)\langle\mathbf{p}_{\mu_w}^{(\nu)}(t')|d_3\boldsymbol{F}(\boldsymbol{\xi}(t'),0,0)\rangle}{\langle\mathbf{p}_{\mu_w}^{(\nu)}|\mathbf{P}_{\mu_w}^{(\nu)}\rangle}b_we^{iwt'}dt'\\=&e^{iwt}b_w\sum_\nu\int_0^\infty e^{(\Gamma^{(\nu)}[\mu_w]-iw)t'}\\&\times\frac{\mathbf{P}_{\mu_w}^{(\nu)}(t)\langle\mathbf{p}_{\mu_w}^{(\nu)}(t-t')|d_3\boldsymbol{F}(\boldsymbol{\xi}(t-t'),0,0)\rangle}{\langle\mathbf{p}_{\mu_w}^{(\nu)}|\mathbf{P}_{\mu_w}^{(\nu)}\rangle}dt',\end{aligned} \tag{D5}$$

where $\langle.|.\rangle$ denotes the usual scalar product and the denominator is time independent, as a standard argument combining the definitions (A1) and (D4) shows. Additionally, the rates $\Gamma^{(\nu)}[\mu_w]$ have negative real part, which follows implicitly from the general theory of differential-difference equations (cf. [20]). Apart from the exponential, the integrand is periodic in t' and by splitting the integration range into intervals of length τ we finally obtain

$$\begin{aligned}\mathbf{r}_w(t)e^{iwt}=&e^{iwt}b_w\sum_\nu\frac{1}{1-e^{\tau\Gamma^{(\nu)}[\mu_w]-iw\tau}}\\&\times\int_0^\tau e^{(\Gamma^{(\nu)}[\mu_w]-iw)t'}\\&\times\frac{\mathbf{P}_{\mu_w}^{(\nu)}(t)\langle\mathbf{p}_{\mu_w}^{(\nu)}(t-t')|d_3\boldsymbol{F}(\boldsymbol{\xi}(t-t'),0,0)\rangle}{\langle\mathbf{p}_{\mu_w}^{(\nu)}|\mathbf{P}_{\mu_w}^{(\nu)}\rangle}dt'.\end{aligned} \tag{D6}$$

The response contains the driving frequency w and integer multiples of the frequency of the orbit $2\pi/\tau$. The spectrum of the control signal $g[\boldsymbol{x}(t)]-g[\boldsymbol{x}(t-\tau)]$ is now easily obtained in linear order. Its amplitude at the driving frequency can be read off from Eq. (D6) and we end up with

$$I(w)=\left|\sum_\nu\frac{(1-e^{-iw\tau})S^{(\nu)}(w)}{1-e^{\tau\Gamma^{(\nu)}[\mu_w]-iw\tau}}\right|^2|b_w|^2, \tag{D7}$$

where

$$S^{(\nu)}(w):=\frac{1}{\tau}\int_0^\tau\int_0^\tau e^{(\Gamma^{(\nu)}[\mu_w]-iw)t'}\frac{\langle Dg[\boldsymbol{\xi}(t)]|\mathbf{P}_{\mu_w}^{(\nu)}(t)\rangle\langle\mathbf{p}_{\mu_w}^{(\nu)}(t-t')|d_3\boldsymbol{F}(\boldsymbol{\xi}(t-t'),0,0)\rangle}{\langle\mathbf{p}_{\mu_w}^{(\nu)}|\mathbf{P}_{\mu_w}^{(\nu)}\rangle}dt'dt \tag{D8}$$

denotes the constant Fourier mode contribution from the periodic orbit. Thus the shape of the spectrum is in general quite complicated. However, the numerators are regular functions of the frequency so that poles, i.e., pronounced line structures in the spectrum, are caused by the zeros of the denominator. If we recall that due to the characteristic equation (6) the expansion

$$\tau\Gamma^{(\nu)}[K(1-e^{-z})]-z = \beta(z-\Lambda\tau-i\Omega\tau)+O[(z-\Lambda\tau-i\Omega\tau)^2] \tag{D9}$$

is valid, we obtain from Eq. (D8) in leading order contributions with Lorentzian line shape, provided the frequency w comes close to the imaginary part Ω of the Floquet exponent and the real part $|\Lambda|$ is small,

$$I(w)\simeq\frac{|(1-e^{-i\Omega\tau})S^{(\nu)}(\Omega)|^2}{|\beta\tau|^2[(w-\Omega)^2+\Lambda^2]}. \tag{D10}$$

Improved expressions for the spectra may be derived by employing, e.g., the linear approximation (A2) in Eq. (D7). But then, for consistency, the frequency dependence of the numerator also has to be taken into account.

[1] K. Pyragas, Phys. Lett. A **170**, 421 (1992).
[2] T. Hikihara and T. Kawagoshi, Phys. Lett. A **211**, 29 (1996).
[3] K. Pyragas and A. Tamasevicius, Phys. Lett. A **180**, 99 (1993).
[4] S. Bielawski, D. Derozier, and P. Glorieux, Phys. Rev. E **49**, R971 (1994).
[5] T. Pierre, G. Bonhomme, and A. Atipo, Phys. Rev. Lett. **76**, 2290 (1996).
[6] T. Bernard, R. Henn, W. Just, E. Reibold, F. Rödelsperger, and H. Benner, in *Nonlinear Microwave Signal Processing: Towards a New Range of Devices*, edited by R. Marcelli (Kluwer, Dordrecht, 1996), p. 373.
[7] W. Just, T. Bernard, M. Ostheimer, E. Reibold, and H. Benner, Phys. Rev. Lett. **78**, 203 (1997).
[8] H. Nakajima, Phys. Lett. A **232**, 207 (1997).
[9] A. Kittel, J. Parisi, and K. Pyragas, Phys. Lett. A **198**, 433 (1995).
[10] W. Just, D. Reckwerth, J. Möckel, E. Reibold, and H. Benner, Phys. Rev. Lett. **81**, 562 (1998).
[11] W. Just, E. Reibold, H. Benner, K. Kacperski, P. Fronczak, and J. Hołyst, Phys. Lett. A **254**, 158 (1999).
[12] W. Just, D. Reckwerth, E. Reibold, and H. Benner, Phys. Rev. E **59**, 2826 (1999).
[13] J.E.S. Socolar, D.W. Sukow, and D.J. Gauthier, Phys. Rev. E **50**, 3245 (1994).
[14] H. Nakajima and Y. Ueda, Phys. Rev. E **58**, 1757 (1998).
[15] H.G. Schuster and M.P. Stemmler, Phys. Rev. E **56**, 6410 (1997).
[16] *Handbook of Chaos Control*, edited by H.G. Schuster (Wiley-VCH, Berlin, 1999).
[17] M.E. Bleich and J.E.S. Socolar, Phys. Lett. A **210**, 87 (1996).
[18] K. Pyragas, Phys. Lett. A **206**, 323 (1995).
[19] R. Bellman and K. L. Cooke, *Differential-Difference Equations* (Academic, New York, 1963).
[20] J. K. Hale and S. M. Verduyn Lunel, *Introduction to Functional Differential Equations* (Springer, New York, 1993).